Experimental Platform for Through-The-Earth Communication

Henrique Berilli Silva Mendes, Adoniran Judson Braga, Josua Daniel Pena Carreno,
Andre Noll Barreto, Leonardo Aguayo, Luis Guilherme Uzeda Garcia*
Dept. of Electrical Engineering of University of Brasilia and Vale Institute of Technology*, Brazil
E-mail: henrique.b.mendes@ieee.org

***Abstract*—This paper presents an experimental software-defined-radio platform for short-range Through-The-Earth (TTE) communication based on magnetic induction. We present a methodology for measurement of channel parameters and of digital communications performance. The obtained results provide data for channel modeling and enable us to find the operational limits in TTE environments.**

***Index Terms*—Magnetic antennas, Through-The-Earth Communications, Extreme Conditions Communications.**

I. Introduction

Several studies have been carried out for estimating the attenuation of Through-The-Earth (TTE) electromagnetic waves for medium and large depths, ranging from tens to hundreds meters, as in [1] and [2]. Those investigations were made to solve the problem of communication with isolated people in underground mines or caves. Nonetheless, little has been mentioned in literature about models or measurement campaigns of signal attenuation for short range TTE communications. Among those limited surveys, Hao and Stevens presented in [3] a buried sensor network, and Akyildiz in [4] proposed a similar system for water-immersed conditions. As an example of short-range TTE applications, some underground assets such as telecommunication cables, gas or water pipes, could transmit data about their operating conditions by the means of TTE communication devices. This data ought be useful for maintenance and replacement planning purposes [3]. Tracking and identifying buried artifacts and explosives are particularly important to the mining industry [5]. For example, in the event of a misfire, the explosives must be safely recovered.

Usually, TTE transmission is performed by magnetic coupling of loop antennas and using low (LF) or very low frequencies (VLF). Such combination can overcome obstacles encountered in the ground [6]. Traditional techniques used in wireless communication, that use radiated electromagnetic waves in the far field zone, do not work properly in this transmission channel due to a great attenuation on field's amplitude in conductive media as in ores and mineral soil. From a practical point of view, the use of low frequencies implies the use of electrically small antennas -which have low radiation efficiency - operating in the near field region [7].

This article presents the project and analysis of a magnetic induction communication system applied to a TTE scenario. Firstly, in Section II we briefly discuss the TTE propagation environment. In Section III we make some considerations on magnetic antennas, and in Section IV we present a channel sounder that measures the channel transfer function in frequency domain and power spectrum density of noise. Additionally, a digital communication link is implemented and its performance is estimated through the BER curve. In Section V, we present and discuss some results and, finally, we make some concluding remarks in Section VI.

II. TTE propagation environment

The penetration of an electromagnetic wave through a conductive medium is not described by the wave equation $\nabla^2 H = \mu\varepsilon(\partial^2 H)/(\partial t^2)$, but by the diffusion equation: $\nabla^2 H = \mu\sigma(\partial H/\partial t)$, where H is the magnetic field within the conductive medium, which is characterized by its conductivity σ, permittivity ε and permeability μ. The decay rate of the electric and magnetic fields within a conductive medium is expressed by the skin depth $\delta = \sqrt{2/(\omega\mu\sigma)}$. That expression permits to infer that reducing the angular frequency w results in increasing the distance at which the medium starts to attenuate the transmitted signal significantly [8]. Additionally, the electromagnetic wave reaching the interface between air and a conductive medium will suffer an alteration of its propagation velocity and wavelength. Considering a transmission through the soil of conductivity of $\sigma = 10^{-3}$ S/m in the LF and VLF bands, the wavelength will experience a reduction of 30 times when compared to air propagation.

A. Magnetic Field Models

In this work, the use of reactive field communication is accomplished by the means of loop antennas used as magnetic transducers. The inductive transmission capability, as a function of the characteristics of a loop antenna, is given by the magnetic moment $m_d = N_{tx} I_{tx} S_{tx}$, where N_{tx} is the number of turns of the transmitting loop, I_{tx} is the RMS value of the electric current at the transmitting antenna, and S_{tx} is the area of the transmitting loop.

Despite the wavelength reduction in conductive media, the antennas are considered as electrically small in near field, and the current is supposed to be uniformly distributed throughout the loop. As a reference for comparison with measurements, we consider in this work the quasi-static (QS) field model

valid for vacuum transmission in homogeneous and uniform medium [9]. We can thus evaluate the excess of propagation loss of measurements in conductive medium in relation to the QS field model. The calculation of time-varying magnetic field strength in QS field hypothesis is made by means of the Biot-Savart law [9], resulting in:

$$\boldsymbol{H}_{qs} = \frac{m_d}{4\pi r^3}\{2\cos(\theta)\,\hat{\boldsymbol{r}} + \sin(\theta)\,\hat{\boldsymbol{\theta}}\} \quad \text{[A/m]}, \tag{1}$$

where $\hat{\boldsymbol{r}}$ and $\hat{\boldsymbol{\theta}}$ are vectors in spherical coordinates in the radial and elevation directions. r represents the distance between the transmitting antenna and the observation location and m_d is the magnetic moment of the transmitting antenna. In coaxial communication, θ equals zero, which is the most practical antenna configuration for TTE communication in vertical direction, so the magnetic field in QS field zone is given by:

$$H_{qs} = \frac{m_d}{2\pi r^3} \quad \text{[A/m]}. \tag{2}$$

B. Channel Modeling

Due to the use of low frequencies, it is more convenient to model the system behavior by using parameters based on the impedance, rather than using scattering parameters. The concept of transfer impedance between loops is adopted, considering the phasor versions of total current in the transmitting loop $I_{tx}\ (\omega)$ and the voltage induced at the receiving antenna terminals $V_{rx}\ (\omega)$. So, its formulation is given by:

$$Z(\omega) = \frac{V_{rx}(\omega)}{I_{tx}(\omega)} \quad [\Omega]. \tag{3}$$

According to Faraday's law [9], the voltage induced by a magnetic field in the terminals of a closed-loop conductor (e.g. a loop antenna) as a function of the magnetic field is given by:

$$\begin{aligned} V_{rx}(\omega) &= -j\omega N_{rx} \oint_S \mu \boldsymbol{H} \cdot \boldsymbol{dS} \\ &= -j\omega\mu N_{rx} S_{rx} H\cos(\varphi) \quad \text{[V]}, \end{aligned} \tag{4}$$

where φ is the angle between the magnetic field vector $\boldsymbol{H}$ and the axis $\hat{\boldsymbol{n}}$ of the loop orthogonal to its plane. Expressing the voltage in spherical coordinates,

$$\begin{aligned} V_{rx}(\omega) = -j\omega\mu N_{rx} S_{rx} \big[&\boldsymbol{H_r}\cos(\theta-\theta_x)\cos(\theta_y)\big] \\ &- \boldsymbol{H_\theta}\sin(\theta-\theta_x)\cos(\theta_y)\big] \quad \text{[V]}, \end{aligned} \tag{5}$$

where θ_x and θ_y are the rotation angles of the x' and y' axes. To understand how those axes work, we must first imagine a local coordinate system at the observation point (center of the receiving antenna), where z' is parallel to z, and x' and y' are computed by rotating z' by $\phi - 90°$, being ϕ the azimuth angle. Figure 1 illustrates the described geometry.

1) Channel transfer function: The antennas are modeled as inductors with very small internal resistance and negligible self-capacitance. The current and voltage are measured at the input of the transmitting antenna and at the terminals of the receiving loop, respectively. To determine the channel transfer function (CTF), the channel impedance $Z_{channel}$ (same as in (3)) is calculated as function of auxiliary quantities. First, we compute the total transfer function F_{total} of the system given by:

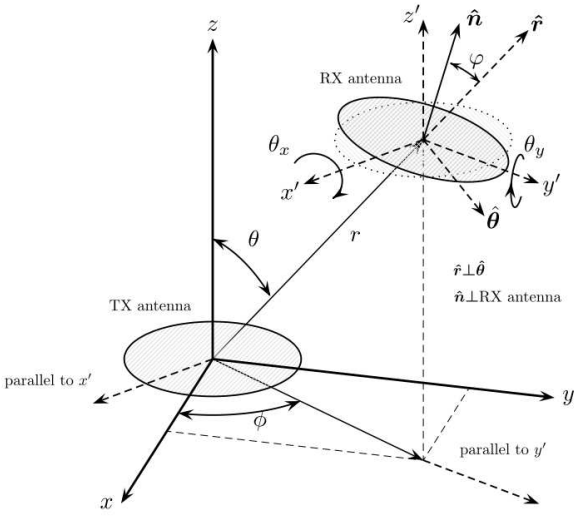

Fig. 1. Geometry for field calculation between two circular Loop antennas.

$$F_{total} = \frac{V_{rx}}{V_{source-tx}}, \tag{6}$$

where $V_{source-tx}$ is the voltage at the output of transmitting amplifier. By measuring the current I_{tx} on the transmitting antenna, it is possible to write:

$$Z_{Channel} = \frac{V_{rx}}{I_{tx}} = \frac{F_{total}\cdot V_{source-tx}}{I_{tx}} = F_{total}\cdot Z_{tx} \quad [\Omega], \tag{7}$$

where Z_{tx} is the input impedance of the transmitting circuit seen by the amplifier. The CTF can be computed by extracting from the $Z_{channel}$ some quantities related to the antennas, as given below:

$$F_{coax} = \frac{Z_{Channel}}{N_{tx}\,N_{rx}\,S_{tx}\,S_{rx}}. \tag{8}$$

For the theoretical calculation of the CTF in the coaxial antennas configuration and in QS field condition, it is necessary to calculate the magnetic field:

$$H_{qs} = \frac{m_d}{2\pi r^3} = \frac{N_{tx}\,S_{tx}\,I_{tx}}{2\pi r^3} \quad \text{[A/m]}. \tag{9}$$

In turn, the induced voltage at the receiving antenna is given, according to Faraday's law, by:

$$\begin{aligned} V_{rx} &= -j\omega\mu N_{rx} S_{rx} H_{qs} \\ &= \frac{-j\omega\mu N_{tx} N_{rx} S_{tx} S_{rx} I_{tx}}{2\pi r^3} \quad \text{[V]}. \end{aligned} \tag{10}$$

Thus, the theoretical CTF is given by:

$$F_{coax} = \frac{-j\omega\mu}{2\pi r^3}. \tag{11}$$

The quasi-static field model was used because it is valid for small distances and frequencies, a scenario that can be easily

configured and measured in laboratory, and used as reference for comparisons with short range TTE measurements.

C. Noise Characteristics

Besides thermal noise, two other kinds of noise are present in frequency bands from ULF to LF, which are usually ignored in the design of conventional communications systems, namely atmospheric noise and man-made noise [10]. The atmospheric noise is modeled as the superposition of a flat and Gaussian background noise and impulsive spikes generated by lightning discharges close to the receiver. The thermal noise is a very important source of noise for higher frequency communication systems, but it is insignificant for our measurements since the antenna aperture is not too small and the atmospheric noise is severe for frequencies below 30 kHz [9]. Amongst man-made noise sources, the harmonic components of electrical power systems are the most relevant. The harmonics are radiated through magnetic and electric fields from electrically powered machines and electrical transmission lines.

Naming the atmospheric and the harmonic noise as external noise and the noise from the amplifier and ADC, both at the acquisition board, as internal noise, we can measure each contribution and evaluate the atmospheric noise temperature. From [9], $F_a = 10\log_{10}(T_a/T_o)$ is a power ratio between the atmospheric and the thermal noise temperature, and is given by:

$$F_a = PSD_a - 20\log_{10}(N_{rx}S_{rx}) - 40\log_{10} f + 492 \ \ [dB]. \tag{12}$$

where PSD_a corresponds to the power spectrum density, in dBV/$\sqrt{\text{Hz}}$, associated to the atmospheric noise computed from voltage measurements.

III. Considerations on Magnetic Antennas

In a scenario where the transmitter and receiver are within the distance range considered as reactive field, the communication is carried out by magnetic coupling.

Usually for TTE communications, the magnetic loop antenna has a circumference less than one-tenth of a wavelength. Thus, there is a relatively constant current distribution along the conductor. Even so, they can reach an area of over 1000 m^2 when used above ground, since their transmission efficiency depends on their absolute size. However, in confined spaces, such as in mines, the use of smaller antennas is mandatory. Such limitation can be compensated by the use of a larger number of coil turns, at the cost of increasing the transmitting antenna impedance and, consequently, the voltage at the amplifier's output.

Resonant circuits are widely used in telecommunication equipment, such as filters and antennas, since they enable the transmission of a certain signal at a given frequency. They operate in a way that the resulting circuit impedance is purely resistive at a frequency where the total reactance is canceled. Radiant antennas have resonant behavior, because they have a resistive and reactive structure. However, antennas that operate far from their resonant frequencies, such as in TTE communications, may require the use of opposite reactors (capacitor, in the case of loop antennas), in order to increase the transmission gain and decrease its operation frequency impedance. For a loop antenna of inductance L, the capacitor needed to produce a maximum gain at frequency f_r is $C_r = (4\pi^2 L f_r^2)^{-1}$.

IV. Experimental Procedure

A. Antennas Manufacturing

The transmitter and receiver antennas have the same square shape and size. Both have 131 cm sides, occupying an area of 1.17 m^2. They were constructed in a cross-shaped wooden support, keeping a square shape during and after the winding of the wire. The transmit antenna has 25 turns with a resistance of 0.53 Ω and inductance of 2.9 mH, while the receiving antenna has 63 turns with a resistance of 1.32 Ω and inductance of 17 mH. These values are from measurements made in the laboratory and are in agreement with the corresponding theoretical calculations within the considered margin of error.

B. Experimental Procedures

Figure 2 summarizes the communication system, either for channel sounding or for digital signal transmission in the SDR based platform. Source and load/acquisition are performed by two independent National Instruments NI USB-6341 boards, and the entire modulation/demodulation and signal processing are realized in real time with the help of one (or two) computers. The measurements were carried out in an underground

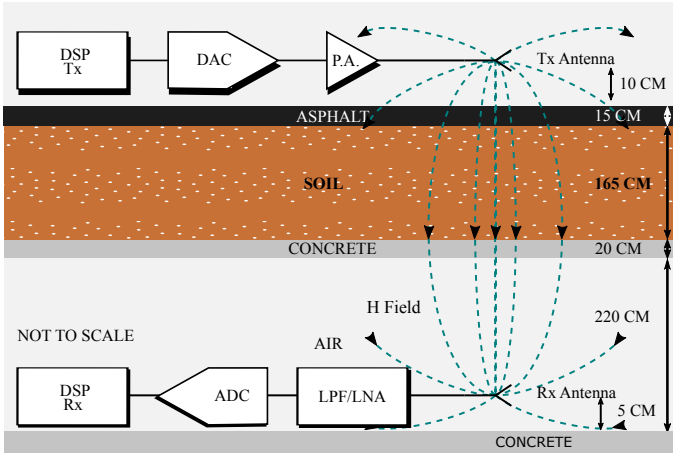

Fig. 2. Block diagram with a TTE transmission scenario.

tunnel that connects the student canteen of the University of Brasilia (RU/UNB) to its steam boiler room. The medium, represented in Figure 2, is composed of layers of air (250 cm), concrete (20 cm), soil (165 cm formed of earth and stones), and asphalt (15 cm). We performed a comparison between the measured data and the theoretical propagation curves in non-conductive medium (air) at 1 m and 4.5 m in the quasi-static field zone. Also, it was compared with a reference measurement carried out at a distance of 1 m through air. The direction of transmission is from surface to underground.

C. Characterization of the Propagation Channel

We use the frequency method to characterize the propagation channel, where N tonal signals sweep the desired band. The complex division between the received and transmitted signal spectra allows us to estimate the channel transfer function. To reduce interference effects by secondary lobes of consecutive tones, a Hanning windowing is employed on time domain.

D. Characterization of the Digital Communication System

We transmit BPSK signals with a 200 bauds symbol rate and transmission bandwidth of 300 Hz at a 5 kHz carrier. This narrow band is usual in TTE communication, because of the preferred resonant circuits with high gain and Q-factor. Other configurations with dumping resistance may be tested in the future to increase the bandwidth at the cost of reducing the power spectrum density of the signal. The baseband signal is raised-cosine filtered with 50% roll-off factor. Channel estimation in frequency domain and zero-forcing (ZF) equalization are implemented for each frame of twenty thousand bits, using 50 pilots per frame, each with a duration equivalent to 16 symbols. Signals are filtered, mixed, summed, up and downconverted, etc. using digital signal processing techniques in a regular SDR platform. No channel coding is used in this test.

V. Results and Discussion

In Figure 3, the channel sounding results are shown through the the TTE channel transfer function, comparing the CTF between surface and underground with the CTF for the QS model at 1 meter and 4.5 meters, and with the CTF measured in air at the reference distance. Analyzing the two upper curves, we see that the reference measurement fits the QS model with a -2.7 dB offset. This difference may be justified by losses at the receiver and its lack of isolation at the measurement environment. This offset is used to calibrate the propagation loss in excess of TTE measurements in comparison to the QS model. By observing the two curves at the bottom of the graph, there is a difference of approximately 4.86 dB of excess loss in addition to the quasi-static model at the frequency of 5 kHz. Subtracting the 2.7 dB from the reference, there is 2.16 dB of excess loss considering the measurement inaccuracies. Comparing measurements for different short ranges to the equivalent QS model may be useful in channel modeling.

Figure 4 displays the channel impedance, taking into account the measured voltage at the receiver and the current passing through the transmitter. This calculation considers the characteristics of the transmit and receive antennas, such as their area and number of turns. When the resonance is used, the gain at each end is computed in the total impedance.

It is observed that the gains in transmission and reception are similar, of around 28 dB, and bandwidth of 200 Hz. The consolidated system gain, for the TTE channel, is approximately 35 dB with a bandwidth of around 150 Hz. At the resonant frequency (5 kHz) it is observed that the total gain equals the sum of the non-resonant channel gain (-21.5 dB),

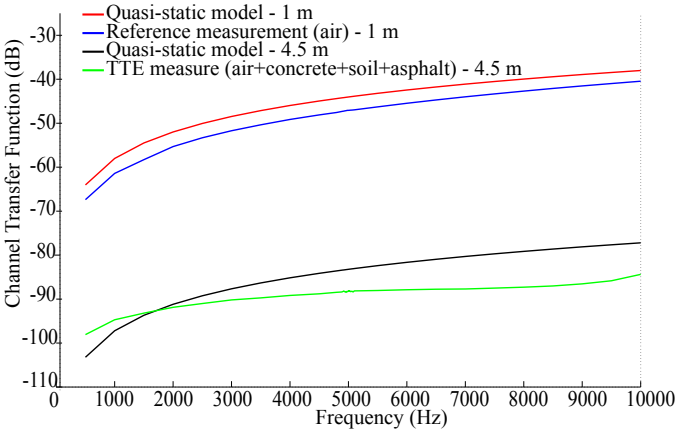

Fig. 3. Channel's Transfer Function (CTF) comparison. Quasi-static model for 1 m and 4.5 m, and measurements at the reference distance and in a short range TTE scenario.

the transmission gain (28 dB), and the reception gain (29 dB). Such addition presents an error of less than 1 dB.

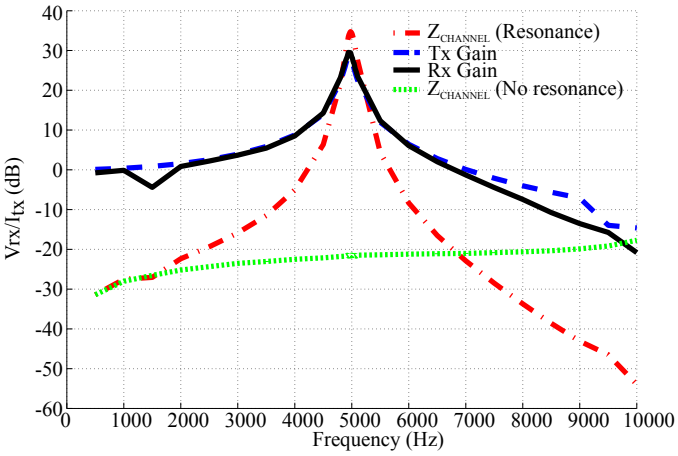

Fig. 4. Experimental Channel's Transfer Impedance, measured according to the setup described at Section IV.

Figure 5 presents the power spectral density of the internal and external noise with and without resonant circuit at the receiving antenna. Ignoring the resonant circuit and harmonic components, the atmospheric noise component in external noise is over 10 dB stronger than internal noise, which is expected for very low frequencies. The strong harmonic components may be explained by the presence of a diesel power generator and industrial steam boilers close to the measurement site. The curve corresponding to the resonant receiver presents higher noise levels with average power spectrum density ($\overline{\text{PSD}}$) of about -70 dBV/$\sqrt{\text{Hz}}$ for some harmonics and -87 dBV/$\sqrt{\text{Hz}}$ for the background noise at 5 kHz. This amplification of noise could discourage the use of the tuning circuit at the receiver, but the use of untuned antenna causes a high-impedance inductive source to the receiver amplifier, which can lead to a high noise voltage if the receiver has a significant input bias current. In other words, the internal noise

could become not so irrelevant as presented in Figure 5.

Observing the middle curve and $\overline{\text{PSD}}$ for 5 kHz we can compute the temperature of atmospheric noise above that of thermal noise using (12). The obtained result of 198 dB is in accordance with the literature, but several measurements with different weather conditions and times are needed.

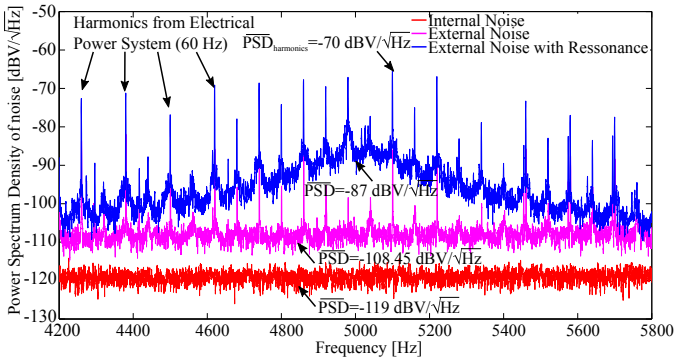

Fig. 5. Experimental Characterization of Noise. Measurements of Power Spectral Density $\overline{\text{PSD}}$ of Receiver's Internal Noise, and External noise for tuned and untuned antennas.

Figure 6 shows the bit error rate as a function of transmit power. It is observed that the transmission power values are low for this scenario. At the BER of 10^{-3}, the current is no more than 260 μA_{RMS}, which is 38 dB below the amplifier's operating limit within its linear zone. This margin guarantees the use of the platform for other short-range scenarios with similar performance.

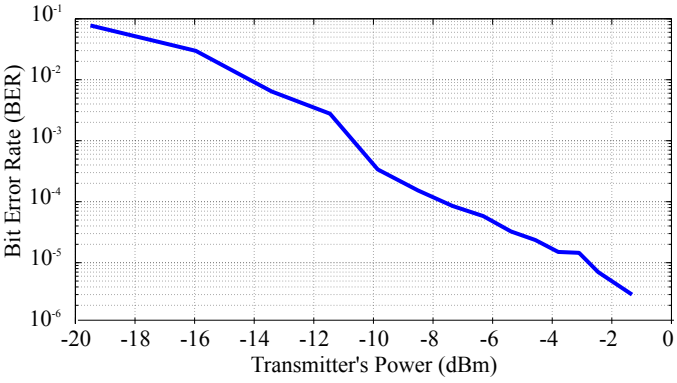

Fig. 6. Bit Error Rate (BER) as a function of transmit power, measured at the receiver output and without channel coding.

VI. Conclusion

In this work, a platform for channel sounding and digital transmission in short range TTE scenarios was presented. The proposed method showed the feasibility of observing some characteristics of the TTE channel and predict and mitigate some of its effects. During the tests, capacitors were coupled to the antenna to study the resonance effect, adding 57 dB of gain in the transmission chain without any active or ohmic component. Based on known models, we could neglect the external noise and verify through measurements that the internal noise contributes to the overall noise thanks to the resonance circuit connected to the antenna. It is important to notice the presence of 5 strong harmonic components within the transmission bandwidth of the digital signal and the linear distortions due to the channel and resonance circuit, resulting in a non AWGN channel. Channel estimation and ZF equalization proved to be essential to achieve reasonable levels of system performance, assessed by measuring BER without channel coding or any technique to mitigate the harmonic components. Further test using different data rates and high-order constellations can be performed using the same experimental platform. The results proved the feasibility of TTE communication at short distances with relatively low power, in the order of -11 dBm for 4.5 m range, with potential applications where buried assets may be connected to transceivers fed by small and long-life batteries.

Acknowledgment

The authors thank the Vale Technological Institute (ITV) for the partnership and financial support for this work and the RU/UNB for allowing access to the measurements site.

References

[1] J. R. Wait, "Electromagnetic induction technique for locating a buried source," *Geoscience Electronics, IEEE Transactions on, vol. 9, no. 2, pp. 95?8*, 1971.

[2] L. Yan, J. A. Waynert, and C. Sunderman, "Measurementsand modeling of through-the-earth communications for coal mines," *IEEE TRANSACTIONS ON INDUSTRY APPLICATIONS, VOL. 49, NO. 5,*, 2013.

[3] T. Hao, H. Burd, D. J. Edwards, and C. J. Stevens, "Enhanced detection of buried assets. in antennas and propagation conference,," *LAPC 2008, Loughborough*, pp. 249–252, 2008.

[4] X. Tan, Z. Sun, and I. F. Akyildiz, "Wireless underground sensor networks: Mi-based communication systems for underground applications." *IEEE Antennas and Propagation Magazine*, vol. 57, no. 4, pp. 74–87, Aug 2015.

[5] E. Isokangas, B. Snmez, M. Wortley, and W. Valery., "Using smarttag to track ore in process integration and optimization projects: some cases studies in a variety of applications." *The Southern African Institute of Mining and Metallurgy Platinum*, 2012.

[6] A. E. Forooshani, "A survey of wireless communications and propagation modeling in underground mines," *Communications Surveys & Tutorials, IEEE, v. 15, n. 4, p. 1524-1545*, 2013.

[7] W. H. Schiffbauer and J. F. Brune, "Underground coal mine communications for emergencies and everyday operation," *Symposium on the Capabilities and Availability of Wireless Communication and Tracking Systems for Underground Coal Mines*, 2006.

[8] D. B. Starkey, "Electromagnetic transmission and detection at deep depths," *Sandia Laboratories Report SLL-73-5278*, 1973.

[9] D. Gibson, *Channel Characterisation and System Design for Sub-Surface Communications*. Ph.D. dissertation, School of Electronic and Electrical Engineering, 2003.

[10] F. H. Raab, "Noise model for low-frequency through-the-earth communication," 2010.